Nanoscale

PAPER

View Article Online
View Journal | View Issue

Cite this: *Nanoscale*, 2018, **10**, 17975

Exciton and phonon dynamics in highly aligned 7-atom wide armchair graphene nanoribbons as seen by time-resolved spontaneous Raman scattering†

Jingyi Zhu, *[a] Raphael German,[a] Boris V. Senkovskiy, [a] Danny Haberer,[b] Felix R. Fischer,[b,c,d] Alexander Grüneis [a] and Paul H. M. van Loosdrecht*[a]

The opening of a band gap in graphene nanoribbons induces novel optical and electronic properties, strongly enhancing their application potential in nanoscale devices. Knowledge of the optical excitations and associated relaxation dynamics are essential for developing and optimizing device designs and functionality. Here we report on the optical excitations and associated relaxation dynamics in surface aligned 7-atom wide armchair graphene nanoribbons as seen by time-resolved spontaneous Stokes and anti-Stokes Raman scattering spectroscopy. On the anti-Stokes side we observe an optically induced increase of the scattering intensity of the Raman active optical phonons which we assign to changes in the optical phonon populations. The optical phonon population decays with a lifetime of ~2 ps, indicating an efficient optical-acoustic phonon cooling mechanism. On the Stokes side we observe a substantial decrease of the phonon peak intensities which we relate to the dynamics of the optically induced exciton population. The exciton population shows a multi-exponential relaxation on the hundreds of ps time scale and is independent of the excitation intensity, indicating that exciton–exciton annihilation processes are not important and the existence of dark and trapped exciton states. Our results shed light on the optically induced phonon and exciton dynamics in surface aligned armchair graphene nanoribbons and demonstrate that time-resolved spontaneous Raman scattering spectroscopy is a powerful method for exploring quasi-particle dynamics in low dimensional materials.

Received 23rd July 2018,
Accepted 13th September 2018

DOI: 10.1039/c8nr05950k

rsc.li/nanoscale

Introduction

Graphene based nanostructures have been attracting widespread attention in research and industry[1–5] since the first graphene electronic device was demonstrated in 2004.[6] Of particular interests are the spatially confined strips of graphene monolayer, dubbed graphene nanoribbons (GNRs). Due to one-dimensional quantum confinement and edge dependent effects, these GNRs display remarkable chemical, electrical and optical properties, including a width tuneable band gap, excitonic optical transition, and potentially room temperature ballistic transport.[7–11] These novel properties result in many potential applications in nanoscale electronic transistor devices,[12,13] optical modulators,[14] quantum gates,[15] and infrared photodetectors.[16,17] The development of applications, as well as the fundamental understanding of the GNRs electronic properties requires knowledge of the fundamental optical excitation properties and energy relaxation mechanisms in these one dimensional systems.

Over the past, electronic structures and excitation properties of GNRs have been investigated *via* conventional spectroscopic techniques such as X-ray absorption,[18,19] scanning tunneling,[20,21] and photoelectron spectroscopy.[22–24] In addition the electronic structure has been studied from a theoretical point of view.[25–28] The general steady state features such as the band gap structure of GNRs are reasonably well understood by now. Studies on the dynamical non-equilibrium properties of GNRs are, however, more scarce most likely due to lack of sufficiently sensitive experimental techniques for these single layered materials. Recently, polarized reflectance measurements combined with *ab initio* calculations[11,29] demonstrated that the optical absorption in armchair

[a]*Physics institute 2, University of Cologne, 50937, Germany. E-mail: jzhu@ph2.uni-koeln.de, pvl@ph2.uni-koeln.de*
[b]*Department of Chemistry, University of California at Berkeley, Tan Hall 699, Berkeley, California 94720, USA*
[c]*Materials Sciences Division, Lawrence Berkeley National Laboratory, Berkeley, CA 94720, USA*
[d]*Kavli Energy NanoSciences Institute at the University of California Berkeley and the Lawrence Berkeley National Laboratory, Berkeley, California 94720, USA*

†Electronic supplementary information (ESI) available. See DOI: 10.1039/c8nr05950k

graphene nanoribbons (AGNRs) are dominated by excitonic transitions. The investigation of the electronic relaxation dynamics in graphene based nanomaterials has been limited to a few cases reporting transient absorption spectroscopy measurements of solution solvated and suspended samples,[30–32] and time resolved terahertz studies of multilayer aggregated GNRs.[33,34] The development of methods to grow aligned GNRs on gold surfaces,[35] and techniques to transfer the GNRs to nonmetallic substrates[36] opened the possibility to study the properties of GNRs in a more controlled manner, including for instance symmetry aspects using polarization sensitive spectroscopies.

Steady state Raman spectroscopy has been proven to be a versatile tool in the characterization of carbon and graphene based materials.[37–39] It allows to determine the number and orientation of layered graphene, yields information on strain, doping, and disorder, and provides a good method to assess the quality of graphene based materials as well as the nature of edges and functional groups in functionalized graphene.[40,41] In addition to this, the time-resolved variant of Raman spectroscopy is a powerful method to investigate both incoherent phonon relaxation as well as electron–phonon coupling and electronic dynamics.[42–49]

In this report, we applied these spectroscopic techniques to study the optical transition properties and in particular the optically induced phonon and electronic dynamics in the 7-atom wide armchair graphene nanoribbons (7-AGNRs) aligned on a silica/silicon substrate. We demonstrated that not only the phonon population, but also the excitonic relaxation dynamics, can be extracted from the optically induced changes in the Raman spectrum. To achieve the latter, we make use of the strong resonant enhancement of the optical phonon Raman scattering due to excitonic transitions. The observed fast phonon creation and relaxation originates from an efficient exciton–phonon and optical–acoustical phonon coupling, respectively, indicating of an efficient energy dissipation in this material. The observed strong resonant optical transition and non-exponential nature of the excitonic relaxation in this one dimensional system evidences the dominated existence of dark and trapped exciton states. These knowledge provide fundamental understanding of the GNRs system toward further optimizing electronic device application.

Experimental

7-AGNRs were synthesized using the well-established bottom-up fabrication approach on Au (788) surfaces which exhibit a regular arrays of narrow (111) terraces dictating the direction of growth[22,35] and yielding high quality, densely aligned ribbons. The transfer from the Au (788) substrate to the insulating silica/silicon substrate was performed by the alignment-preserving bubbling transfer method based on an electrochemical delamination process.[36,50,51] The bottom up syntheses process and our sample transfer method guarantees that we have monolayer 7-AGNRs film.[52]

Steady state (one laser beam) Raman spectra of 7-AGNRs were performed using a micro-Raman setup equipped with a tandem triple spectrometer (Spectroscopy & Imaging GmbH) and LN_2 cooled CCD (PyLoN 100; Princeton Instruments). An optical parametric amplifier (OPA, Light conversion), pumped by a single-unit amplified femtosecond laser (Pharos, Light conversion) running at a repetition rate of 100 kHz provided wavelength tunable (400 nm to 800 nm; 1.5–3.1 eV) picosecond pulses (~2 ps) as excitation source. The excitation pulses were spectrally cleaned and narrowed (full width a half maximum (FWHM) ~10 cm^{-1}) using a home build pulse shaper. The pulses were focused on the sample with a 20 times micro objective, and Raman signals were collected in a backscattering geometry. To avoid sample degradation, samples were mounted in a cryostat pumped down to 10^{-5} mbar.

Time-resolved measurements (Fig. 1a) of 7-AGNRs were performed with the same setup by introducing a pump laser pulse (~300 fs) provided by a second OPA (ORPHEUS, Light conversion) pumped by the same amplified laser. Details of the time-resolved spontaneous Raman spectroscopy technics and methods have been described elsewhere.[53] The samples were pumped with laser wavelengths of 590 nm (2.1 eV) and 490 nm (2.5 eV) respectively, and Raman signal were collected using 512 nm (2.4 eV) probe pulses (Fig. 1c). Both the pump and probe light polarization are parallel to the long axis of the AGNRs. In order to avoid optical damage of the samples and improve the signal to noise ratio, the laser spot sizes on the

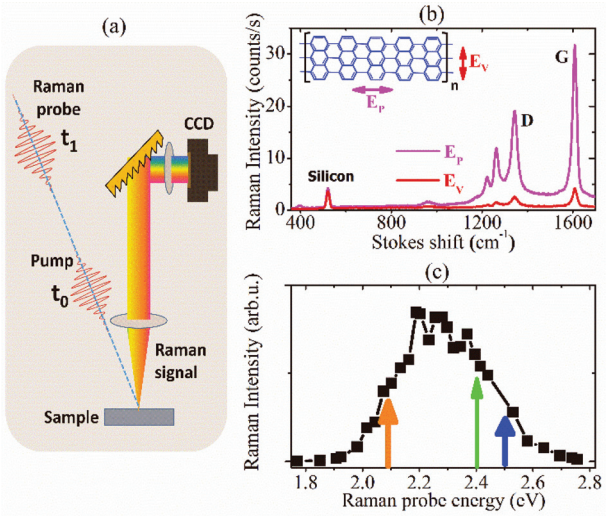

Fig. 1 (a) Illustration of the spontaneous Raman scattering experiments. Steady state measurement is obtained when the pump beam is blocked. (b) Steady state Raman scattering spectra of the 7-AGNRs on silica/silicon recorded with picosecond pulsed laser at 512 nm, E_P indicates that the polarization of laser pulse is along the ribbons, E_V indicates that the polarization of laser pulse perpendicular to the ribbons. (c) Energy dependence of the Raman intensity of the phonon G peak, showing a strong resonant enhancement of the Raman scattering. Dark yellow and blue arrows indicate the pump energies used for the time-resolved experiments, green arrow indicates the Raman probe energy used for the data shown in (a) and for the time-resolved experiments.

sample were defocused to ~60 μm. The back reflected Raman scattering signals were re-collimated with an additional telescope lens group before entering the spectrometer. Time-resolved measurements were performed using pump pulse fluencies ranging from 7.5 μJ cm^{-2} (0.47×10^{14} photons per cm^2) to 38.2 μJ cm^{-2} (2.37×10^{14} photons per cm^2). Under these conditions no signs of damage to the sample are observed after hours of measuring. At higher fluencies (>50 μJ cm^{-2}) we observed a slow ingrowth of a broad band 'background' signal with time and a slowly decreasing phonon peak intensity indicating damage to the sample.

Results and discussion

Fig. 1b presents typical steady state polarized Raman scattering spectra of the 7-AGNRs on Stokes side. The phonon scattering peak at around 521 cm^{-1} originates from the silica/silicon substrate and provides a good reference for the measurements. The highly orientated nature of our samples is demonstrated by the strong enhancement (~10×) of the Raman signal when the incoming light is polarized along the ribbons.[36] The G- and D-like modes typical for all graphene related materials are clearly observed in the spectra. The C–C stretching G-like mode, located at 1608 cm^{-1}, corresponds to a carbon–carbon bond stretching mode along the ribbon. The D-like mode related to the armchair edge termination of GNRs[54] is found at 1345 cm^{-1} and is weaker than the G-like mode. Other vibrational Raman peaks,[55] like the breathing mode related to the ribbon width expansion is found at 398 cm^{-1}, and the confinement derived vibrational modes at 1255 cm^{-1} and 1266 cm^{-1} were also well resolved. In general, the spectra measured with the pulsed laser are fully consistent with previous results measured on 7-AGNRs on insulating and metallic substrate surface[36,56] with continuum lasers.

To investigate resonance effects due to optical transitions in 7-AGNRs, wavelength dependent Raman scattering measurements were performed. Fig. 1c depicts the resonance profile of the integrated intensity of the G-like mode (for the spectra see Fig. S1†). A clear resonant profile was observed, centered at ~2.3 eV with a FWHM of ~0.4 eV. The observed resonant profile resembles the imaginary part of the dielectric function of 7-AGNRs on a gold substrate, which was interpreted in terms of an excitonic transition.[11] The excitonic transition width observed here with Raman is much broader than those of nanotubes, the reason for this most likely originate from the fact that two electronic transitions (E_{11} and E_{22}) are involved[11] combined with inhomogeneous broadening due to a broad length distribution[22] and possibly defects induced in the sample transfer process. The fundamental energy gap for 7-AGNRs on a gold surface is strongly reduced due to polarization screening by the substrate compared to the theoretically calculated energy gap of ~3.7 eV.[11] In our case one expects a much weaker screening by the silica/silicon substrate, and hence a substantially higher single particle band gap. Indeed, it has been demonstrated that the reduced screening for 7-AGNRs aligned on an Au–silicon alloy substrate leads to a band gap of 2.7 eV.[57] Since the dielectric constant of our silica/silicon substrate is even lower, we expect a single particle band gap much closer to the theoretical value of 3.7 eV. In view of this we can safely assign the observed resonance around 2.3 eV in the Raman scattering experiment to excitonic transitions associated with an exciton binding energy larger than 1 eV.

Fig. 2a depicts the time-resolved Stokes spectra after optical excitation at 590 nm (2.1 eV), with excitation laser intensity around 1.2×10^{14} photons per cm^2. To more clearly exhibit the pump induced effects on the Raman spectra, Fig. 2b shows difference spectra obtained by subtracting the −5 ps spectrum (top panel Fig. 2a) from the time delayed spectra in Fig. 2a. As is clear from the figures, the Raman spectra show an overall decrease of scattering intensity for all time delays, which recovers on a hundreds of ps time scale. Similar spectral changes were also observed upon excitation at higher photon energy at 490 nm (2.5 eV) (Fig. S2†). These observations contrast the usual observations in time-resolved spontaneous Raman experiments of an increasing optical phonon scattering intensity originates from an, through the electron–phonon scattering processes, optically increased phonon population.[45,48,58] This surprising result can be understood in terms of optically induced changes in the Raman resonance efficiency which allows extraction of the electronic relaxation dynamics from our data, as we will elaborate later on in this report.

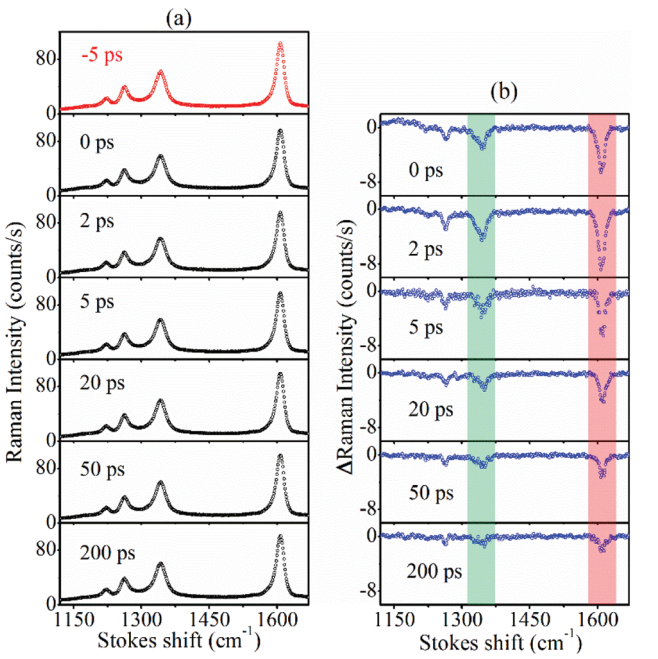

Fig. 2 Time-resolved spontaneous Raman scattering spectra of the 7-AGNRs recorded on Stokes side, with pump energy at 2.1 eV and Raman probe energy at 2.4 eV. (a) Raman scattering intensity spectra at different delay times after optical excitation. (b) Difference spectra obtained by subtraction the spectrum at −5 ps from each spectrum in (a) at different corresponding delay time. The color bars indicate the integration regions used in the analysis of the transient behaviour.

To obtain a more detailed insight into the dynamics, the changes in the phonon scattering intensities of the D-like and G-like bands are integrated (over regions indicated by the colored areas in Fig. 2b) for each time delay. The dynamics of the D-like and G-like bands are plotted in Fig. 3 and are found to be identical: the changes in the Stokes spectra show a substantial decay within 100 s of ps, but only fully recover on a ns time scale, which is out of our detection window. Multi-exponential decay functions are required to fit the data, where a global fitting of the D-like and G-like responses yield decay times of 1.4 ps and 34 ps for the 2.1 eV pumped spectra, and 1.7 and 37 ps for the 2.5 eV pumped spectra. The 20–40 ps decay dynamics observed is much longer than the general optical phonon population dynamics in graphite and graphene related systems[44,45,48,49,58] which are in the time range of 1–2 ps. On the other hand, the lifetime constants obtained here are comparable to those of dynamics in various graphene nanotubes,[59–62] where the excitons dynamics typically shows a double exponential decay with lifetimes of 1–15 ps and 30–90 ps, respectively. This, together with the resonant nature of the Raman scattering, strongly suggests that an exciton related relaxation mechanism is responsible for the observations.

To test if any many-body relaxation mechanisms are involved in the decay of the Stokes response, excitation intensity dependent measurements are carried out with the pump photon energy at 2.1 eV. The measured results are presented in Fig. 4. Since dynamics form D-like and G-like peaks are generally the same, only the average of the D-like and G-like responses is plotted. For pump excitation densities $<2 \times 10^{14}$ photons per cm^2 a linear increase of the signal is observed which seems to saturate above this value (see inset in Fig. 4a). Fig. 4b, which shows the same data normalized to the maximum response, indicates that there is no pump excitation power dependence in the dynamics, demonstrating the absence of many-body processes in the transient behavior of the signal.

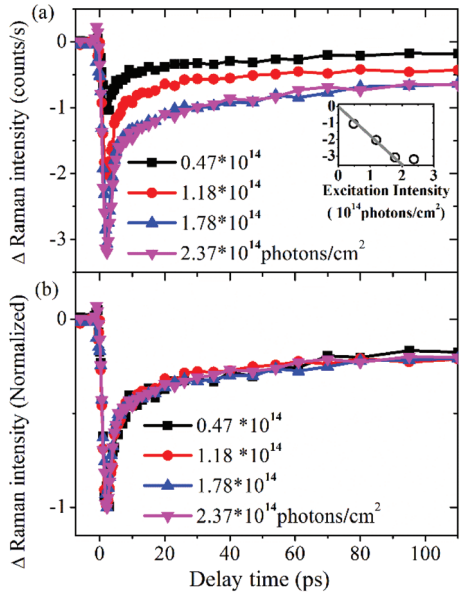

Fig. 4 Pump (2.1 eV) excitation intensity dependence of the decay dynamics. The data represent the averaged response of the D-like and G-like bands. In (a) the raw data are presented and in (b) data are normalized to show the absence of the pump intensity dependent dynamics. The inset in (a) shows the pump excitation intensity dependence of the amplitude at a delay of 2 ps.

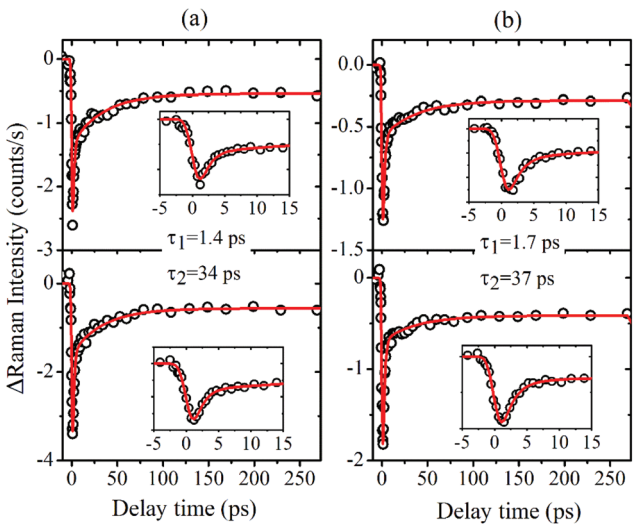

Fig. 3 Decay dynamics of the phonon peak D-like (top panels) and G-like (bottom panels). (a) Dynamics observed at the excitation wavelength of 590 nm (2.1 eV). (b) Dynamics observed at the excitation wavelength of 490 nm (2.5 eV). Black circles represent the experimental data, red lines represent a global fitted. Insets show the short time dynamics.

It is clear from the above that the dynamics of the phonon population cannot be extracted from the Stokes side Raman spectra. In order to obtain insight in the phonon population dynamics we have therefore carried out time-resolved experiments on anti-Stokes side, using identical experimental conditions with a pump energy of 2.1 eV and pump intensity of 1.2×10^{14} photons per cm^2. The recorded time dependent spectra are presented in Fig. 5, in the same manner as those on Stokes side in Fig. 2. Indeed a pump induced enhancement of the phonon scattering signals is observed for both D-like and G-like responses on the anti-Stokes side. The dynamics show a very fast response, with ingrowth times faster than our time resolution and decay time of ~2 ps. The integrated intensity dynamics for the D-like and G-like responses in Fig. 5(a) are shown in Fig. 6(a), both have identical relaxation dynamics. A global single exponential fit yields a decay constant of 1.9 ps, which can be interpreted as the lifetime of the optical phonons.

In principle, phonon temperatures[63,64] can be obtained from the signal ratio between Stokes and anti-Stokes side, based on the detailed balance resulted from fluctuation–dissipation theorem. However, due to the strong resonance Raman effects this is not trivial. We therefore estimated the transient optical phonon temperature using the reasonable assumption (ESI†) that before time zero the phonon temperatures are

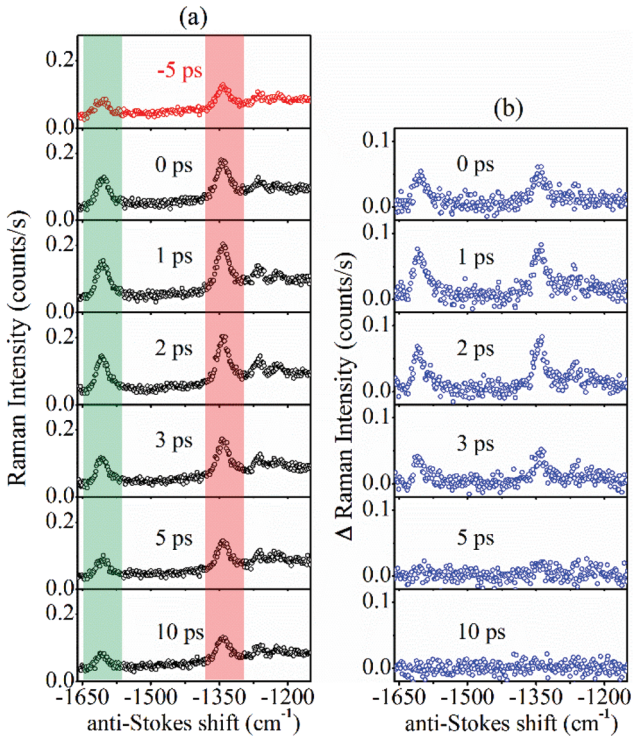

Fig. 5 Time-resolved spontaneous Raman scattering spectra of the 7-AGNRs recorded on anti-Stokes side. (a) Raman scattering intensity spectra at different delay times after optical excitation at 2.1 eV. (b) Pump induced difference spectra obtained by subtraction the spectrum at −5 ps from each spectrum in (a) at different corresponding delay times.

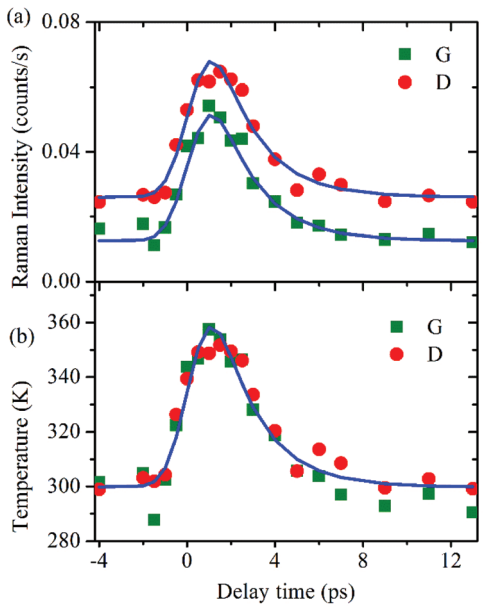

Fig. 6 Phonon population dynamics of 7-AGNRs extracted from anti-Stokes spectra. (a) Dynamics for peak D- and G-like (symbols: experimental data; lines: globe single exponential fit). (b) Calculated D- and G-like transient phonon temperatures.

equal to the environment temperature (~300 K). As indicated in Fig. 6(b), the transient temperatures estimated from both D-like and G-like peaks are, within the experimental accuracy, identical and reach a maximum value of 350 K within our time resolution. They decay to the equilibrium temperature within 2 ps as the optical phonons are depopulated through optical-acoustical phonon scattering.

As have been observed from the dynamics of the optical phonon peaks D-like and G-like, the decay behaviors on anti-Stokes side matches the phonon population dynamics, while the decay behaviors on Stokes side matches the electronic relaxation time scale in graphene based materials. To further clearly derive these relations, we assume that the pump induced phonon signal changes are contributed by both of the phonon population and the Raman susceptibility changes. Ignoring other constant parameters, simply the observed Raman signals on the Stokes side[65] can be expressed as:

$$I^{s}_{\text{un-pumped}} = |\chi_R|^2\ (1 + n_p) \tag{1}$$

where χ_R is the phonon Raman susceptibility tensor and n_p is the statistical phonon population number. After optical excitation, the time dependent change of $|\chi_R|^2$ and n_p is $\Delta|\chi_R|^2(t)$ and $\Delta n_p(t)$ respectively. Thus Raman signal after optical excitation is:

$$I^{s}_{\text{pumped}} = [|\chi_R|^2 + \Delta|\chi_R|^2(t)]\ [1 + n_p + \Delta n_p(t)] \tag{2}$$

such that the pump induced difference signal is

$$\begin{aligned}\Delta I^{s}(t) &= I^{s}_{\text{pumped}} - I^{s}_{\text{un-pumped}} \\ &= [|\chi_R|^2 + \Delta|\chi_R|^2(t)]\ \Delta n_p(t) + (1 + n_p)\ \Delta|\chi_R|^2(t)\end{aligned} \tag{3}$$

Since $\Delta n_p(t) \ll 1$ and $n_p \ll 1$, formula (3) can be reduced to

$$\Delta I^{s}(t) = \Delta|\chi_R|^2(t) \tag{4}$$

Clearly this indicates that the signal changes on Stokes sides are dominated by the Raman tensor changes. The decreasing of Raman susceptibility can easily be understood from resonant properties of the Raman process, based on a two-state mode. Since the resonant Raman scattering signals are dictated by the first step of resonant optical transition, a bleach of the electronic ground state, or state filling on the excited state, can decrease the optical transition probabilities and thus reduces the Raman signals. For a simplified two energy level model system, we demonstrate that the Raman tensor square changes has simple relation to the hole population probability (ESI†) ρ, written as:

$$\Delta|\chi_R|^2(t) = -4\kappa^2\rho \tag{5}$$

where κ is a constant, related to the optical transition matrix elements involved in the Raman process. Thus (4) becomes:

$$\Delta I^{s}(t) = -4\kappa^2\rho \tag{6}$$

which indicates that, on the Stokes side, the difference signal observed is linearly related to the electron (hole) density.

Therefore, the observed decay of Raman signals can be attributed to the electronic relaxation dynamics.

Similarly, on anti-Stokes side, the pump induced difference signal can be expressed as:

$$\begin{aligned}\Delta I^{\mathrm{as}}(t) &= \Delta n_{\mathrm{p}}(t)\ |\chi_{\mathrm{R}}|^2 + n_{\mathrm{p}}\Delta|\chi_{\mathrm{R}}|^2(t) + \Delta n_{\mathrm{p}}(t)\ \Delta|\chi_{\mathrm{R}}|^2(t) \\ &= n_{\mathrm{p}}|\chi_{\mathrm{R}}|^2[\Delta n_{\mathrm{p}}(t)/n_{\mathrm{p}} + \Delta|\chi_{\mathrm{R}}|^2(t)/|\chi_{\mathrm{R}}|^2 \\ &+ \Delta n_{\mathrm{p}}(t)\Delta|\chi_{\mathrm{R}}|^2(t)/n_{\mathrm{p}}|\chi_{\mathrm{R}}|^2]\end{aligned} \quad (7)$$

In a condition that the phonon population $\Delta n_{\mathrm{p}}(t)$ induced by the pump is larger comparing to the equilibrium phonon population n_{p}, while $\Delta|\chi_{\mathrm{R}}|^2$ is only a few percent of $|\chi_{\mathrm{R}}|^2$ (which is true for most of experiments), *i.e.* specifically we have

$$\Delta n_{\mathrm{p}}(t)/n_{\mathrm{p}} \gg \Delta|\chi_{\mathrm{R}}|^2(t)/|\chi_{\mathrm{R}}|^2 \quad (8)$$

Thus the last two terms on the right side of (7) can be ignored, and (7) reduces to

$$\Delta I^{\mathrm{as}}(t) = |\chi_{\mathrm{R}}|^2\ \Delta n_{\mathrm{p}}(t) \quad (9)$$

This is exactly the expected result for the phonon population dynamics which can be observed from anti-Stokes side and is proportional to the signal intensity changes. From above simple analysis, we conclude here that in time-resolved spontaneous Raman spectroscopy, phonon and electronic population dynamics can be observed from the anti-Stokes and Stoke side Phonon signal changes respectively.

The optical phonons life time (~2 ps) in 7-AGNRs is found to be very similar to the dynamics observed in graphite and graphene nanotubes.[48,58] The main difference is in the observed temperature increase which is only 50 K in 7-AGNRs and can exceed 1000 K in graphite under similar excitation conditions.[48] Correspondingly, the phonons in 7-AGNRs also do not show any spectral dynamics such as the stiffening observed in graphite. These differences originate from the generation mechanism of the optical phonons. In the experiments on graphite the optically induced phonon population is created through relaxation of the highly excited free carriers to the conduction band minimum. In our experiments on the 7-AGNRs, however, the optical transitions are excitonic in nature and excited with only a limited amount of excess energy (*i.e.* close to resonant excitation), leading to a much lower raise of the phonon population, and thus phonon temperature, as compared to the graphite case.

The most interesting observation reported here is arguably the decay dynamics of the Stokes spectra. Since we are directly exciting the excitonic transition responsible for the resonant Raman enhancement, the transient decay of the Stokes response directly reflects the exciton dynamics of the 7-AGNRs (see ESI†). The reduction of the resonant enhancement is a direct consequence of ground state bleaching/excited state filling, *i.e.* of the reduction of the optical transition probability. We note that pump–probe Terahertz conductivity experiments on multi-layered AGNRs[34] showed a short lived dynamics (1–2 ps) which has been assigned to free carrier relaxation followed by the formation of excitons. Though we observe a similar fast time scale of the initial decay of the Stokes response, its origin has a different nature. Our steady state resonant Raman results demonstrate the pure excitonic nature of the transitions around 2.3 eV in 7-AGNRs, therefore one does not expect any substantial density of free carriers directly after pump excitation. This is corroborated by the observation that the dynamics and amplitudes of the signal are nearly identical for both excitation energies used in the experiments (2.1 eV and 2.5 eV, see Fig. 3), and by the observation that the fast decay components recovers around 50% of the initial amplitude. The latter would not be expected if formation of excitons from free carriers is responsible for the initial fast decay since such a process does not substantially recover the optically induced ground state bleaching and thus the changes in the Raman resonance enhancement.

Since 7-AGNRs are non-luminescent,[36] exciton recombination must be a non-radiative decay process. In carbon nanotubes, non-radiative exciton relaxation decay proceeds by passing through either long-lived defect related trap states,[66] or through scattering into the optically inactive dark exciton states.[67] Similarly in the AGNRs, one expects both trap and dark states. The dark states are derived from the E_{12} (upper valence band to second conduction band) and E_{21} (second valence band to lowest conduction band) transitions,[25,26] whereas defect related trap states (both short and long lived) are expected to be present either originating from the bottom up growth process or from the electrochemical transfer process. The observed decay dynamics can now be understood as follows. After the initial creation of the free exciton population excitons populate both dark as well as trap states. Within the first 2 ps part of this population (short lived trap states) recombine, thereby reducing the transient response. In the following 30 ps dark excitons decay non-radiatively, leaving only the long lived trap exciton states, which amount to about 20% of the initial excited exciton population. These latter then decay on a nanosecond timescale which is out of our observation window.

In most graphene based nanomaterials, such as the carbon nanotubes[68–70] and a cove-shaped graphene nanoribbons,[30] diffusion controlled exciton–exciton annihilation dominates the exciton relaxation processes. Our experiments have shown that in our case many-body processes do not play a dominant role. This is understandable in view of the relatively short length[22] of the 7-AGNRs (~20 nm) compared to carbon nanotubes (exceeding 1 μm) and the mild excitation conditions used in our experiments: one does not expect a substantial amount of AGNRs with more than one exciton excited and hence no exciton–exciton annihilation process occurs.

Conclusion

In summary, we have employed time-resolved spontaneous Raman spectroscopy to reveal the absence of exciton–exciton annihilation processes and a peculiar dependence of the Raman

intensity on the Raman tensor for Stokes and anti-Stokes sides in 7-AGNRs. Optical excitation of the excitonic transitions leads to an enhanced optical phonon population through relaxation of the excess exciton energy by exciton–phonon scattering on a time scale faster than our temporal resolution (~1.5 ps). The decay times of the optical D-like and G-like phonon populations, originating from optical-acoustic phonon scattering, are found to be ~2 ps, similar to values found in other graphene based nanomaterials and graphite. The exciton dynamics is directly reflected in the optical induced changes of Raman susceptibility. No evidence for diffusion controlled exciton–exciton recombination has been found, consistent with expectations. The exciton relaxation is found to be multi-exponential (decay constants ~1.5, ~30 ps and >1 ns) reflecting the presence of short and long lived trap states as well as the expected dark states with a life time of ~30 ps.

Conflicts of interest

There are no conflicts to declare.

Acknowledgements

Financial support by the Deutsche Forschungsgemeinschaft (DFG) through CRC1238 (projects B05 and A01) and project INST 216/798-1 is gratefully acknowledged. U.S. Department of Energy (DOE), Office of Science, Basic Energy Sciences (BES) under award no. DE-SC0010409 (precursor synthesis and characterization). A. G. and B. S. acknowledge the ERC grant no. 648589 'SUPER-2D'.

Notes and references

1 A. Narita, X. Y. Wang, X. L. Feng and K. Müllen, *Chem. Soc. Rev.*, 2015, **44**, 6616–6643.
2 M. J. Allen, V. C. Tung and R. B. Kaner, *Chem. Rev.*, 2010, **110**, 132–145.
3 F. Bonaccorso, Z. Sun, T. Hasan and A. C. Ferrari, *Nat. Photonics*, 2010, **4**, 611–622.
4 P. Avouris and M. Freitag, *IEEE J. Sel. Top. Quantum Electron.*, 2014, **20**, 6000112.
5 A. N. Enyashin and A. L. Ivanovskii, *Phys. Status Solidi B*, 2011, **248**, 1879–1883.
6 K. S. Novoselov, A. K. Geim, S. V. Morozov, D. Jiang, Y. Zhang, S. V. Dubonos, I. V. Grigorieva and A. A. Firsov, *Science*, 2004, **306**, 666–669.
7 K. Wakabayashi, K. Sasaki, T. Nakanishi and T. Enoki, *Sci. Technol. Adv. Mater.*, 2010, **11**, 054504.
8 J. Alfonsi and M. Meneghetti, *New J. Phys.*, 2012, **14**, 053047.
9 J. Baringhaus, M. Ruan, F. Edler, A. Tejeda, M. Sicot, A. Taleb-Ibrahimi, A. P. Li, Z. G. Jiang, E. H. Conrad, C. Berger, C. Tegenkamp and W. A. de Heer, *Nature*, 2014, **506**, 349–354.
10 J. J. Palacios, *Nat. Phys.*, 2014, **10**, 182–183.
11 R. Denk, M. Hohage, P. Zeppenfeld, J. Cai, C. A. Pignedoli, H. Söde, R. Fasel, X. Feng, K. Müllen, S. Wang, D. Prezzi, A. Ferretti, A. Ruini, E. Molinari and P. Ruffieux, *Nat. Commun.*, 2014, **5**, 4253.
12 F. Schwierz, *Nat. Nanotechnol.*, 2010, **5**, 487–496.
13 M. C. Lemme, T. J. Echtermeyer, M. Baus and H. Kurz, *IEEE Electron Device Lett.*, 2007, **28**, 282–284.
14 H. Zhang, Y. Miyamoto, X. L. Cheng and A. Rubio, *Nanoscale*, 2015, **7**, 19012–19017.
15 I. G. Karafyllidis, *J. Comput. Sci.*, 2015, **11**, 326–330.
16 E. Ahmadi, A. Asgari and K. Ahmadiniar, *Superlattices Microstruct.*, 2012, **52**, 605–611.
17 E. Ahmadi and A. Asgari, *Phys. Scr.*, 2013, **T157**, 014003.
18 X. H. Zhu, A. P. Hitchcock, C. Bittencourt, P. Umek and P. Krüger, *J. Phys. Chem. C*, 2015, **119**, 24192–24200.
19 P. Guttmann, C. Bittencourt, S. Rehbein, P. Umek, X. X. Ke, G. Van Tendeloo, C. P. Ewels and G. Schneider, *Nat. Photonics*, 2012, **6**, 25–29.
20 H. Söde, L. Talirz, O. Gröning, C. A. Pignedoli, R. Berger, X. L. Feng, K. Müllen, R. Fasel and P. Ruffieux, *Phys. Rev. B: Condens. Matter Mater. Phys.*, 2015, **91**, 045429.
21 A. Kimouche, M. M. Ervasti, R. Drost, S. Halonen, A. Harju, P. M. Joensuu, J. Sainio and P. Liljeroth, *Nat. Commun.*, 2015, **6**, 10177.
22 S. Linden, D. Zhong, A. Timmer, N. Aghdassi, J. H. Franke, H. Zhang, X. Feng, K. Müllen, H. Fuchs, L. Chi and H. Zacharias, *Phys. Rev. Lett.*, 2012, **108**, 216801.
23 P. Ruffieux, J. M. Cai, N. C. Plumb, L. Patthey, D. Prezzi, A. Ferretti, E. Molinari, X. L. Feng, K. Müllen, C. A. Pignedoli and R. Fasel, *ACS Nano*, 2012, **6**, 6930–6935.
24 A. Della Pia, G. Avvisati, O. Ourdjini, C. Cardoso, D. Varsano, D. Prezzi, A. Ferretti, C. Mariani and M. G. Betti, *J. Phys. Chem. C*, 2016, **120**, 7323–7331.
25 L. Yang, M. L. Cohen and S. G. Louie, *Nano Lett.*, 2007, **7**, 3112–3115.
26 D. Prezzi, D. Varsano, A. Ruini, A. Marini and E. Molinari, *Phys. Rev. B: Condens. Matter Mater. Phys.*, 2008, **77**, 040404.
27 X. Zhu and H. B. Su, *J. Phys. Chem. C*, 2010, **114**, 17257–17262.
28 X. Zhu and H. B. Su, *J. Phys. Chem. A*, 2011, **115**, 11998–12003.
29 R. Denk, A. Lodi-Rizzini, S. Wang, M. Hohage, P. Zeppenfeld, J. Cai, R. Fasel, P. Ruffieux, R. F. J. Berger, Z. Chen, A. Narita, X. Feng, K. Müllen, R. Biagi, V. De Renzi, D. Prezzi, A. Ruini and A. Ferretti, *Nanoscale*, 2017, **9**, 18326–18333.
30 G. Soavi, S. Dal Conte, C. Manzoni, D. Viola, A. Narita, Y. B. Hu, X. L. Feng, U. Hohenester, E. Molinari, D. Prezzi, K. Müllen and G. Cerullo, *Nat. Commun.*, 2016, **7**, 11010.
31 Z. P. Zhu, J. Crochet, M. S. Arnold, M. C. Hersam, H. Ulbricht, D. Resasco and T. Hertel, *J. Phys. Chem. C*, 2007, **111**, 3831–3835.
32 J. Chmeliov, J. Narkeliunas, M. W. Graham, G. R. Fleming and L. Valkunas, *Nanoscale*, 2016, **8**, 1618–1626.

33 S. A. Jensen, R. Ulbricht, A. Narita, X. L. Feng, K. Müllen, T. Hertel, D. Turchinovich and M. Bonn, *Nano Lett.*, 2013, **13**, 5925–5930.
34 Z. P. Chen, H. I. Wang, J. Teyssandier, K. S. Mali, T. Dumslaff, I. Ivanov, W. Zhang, P. Ruffieux, R. Fasel, H. J. Räder, D. Turchinovich, S. De Feyter, X. L. Feng, M. Kläui, A. Narita, M. Bonn and K. Müllen, *J. Am. Chem. Soc.*, 2017, **139**, 3635–3638.
35 J. M. Cai, P. Ruffieux, R. Jaafar, M. Bieri, T. Braun, S. Blankenburg, M. Muoth, A. P. Seitsonen, M. Saleh, X. L. Feng, K. Müllen and R. Fasel, *Nature*, 2010, **466**, 470–473.
36 B. V. Senkovskiy, M. Pfeiffer, S. K. Alavi, A. Bliesener, J. Zhu, S. Michel, A. V. Fedorov, R. German, D. Hertel, D. Haberer, L. Petaccia, F. R. Fischer, K. Meerholz, P. H. van Loosdrecht, K. Lindfors and A. Grüneis, *Nano Lett.*, 2017, **17**, 4029–4037.
37 A. C. Ferrari and J. Robertson, *Philos. Trans. R. Soc., A*, 2004, **362**, 2269–2270.
38 A. C. Ferrari, *Solid State Commun.*, 2007, **143**, 47–57.
39 A. C. Ferrari and J. Robertson, *Philos. Trans. R. Soc., A*, 2004, **362**, 2477–2512.
40 A. C. Ferrari and D. M. Basko, *Nat. Nanotechnol.*, 2013, **8**, 235–246.
41 C. Neumann, S. Reichardt, P. Venezuela, M. Drögeler, L. Banszerus, M. Schmitz, K. Watanabe, T. Taniguchi, F. Mauri, B. Beschoten, S. V. Rotkin and C. Stampfer, *Nat. Commun.*, 2015, **6**, 8429.
42 J. A. Kash, J. C. Tsang and J. M. Hvam, *Phys. Rev. Lett.*, 1985, **54**, 2151–2154.
43 K. T. Tsen and H. Morkoc, *Phys. Rev. B: Condens. Matter Mater. Phys.*, 1988, **38**, 5615–5616.
44 K. Kang, T. Ozel, D. G. Cahill and M. Shim, *Nano Lett.*, 2008, **8**, 4642–4647.
45 D. H. Song, F. Wang, G. Dukovic, M. Zheng, E. D. Semke, L. E. Brus and T. F. Heinz, *Phys. Rev. Lett.*, 2008, **100**, 225503.
46 D. Fausti, O. V. Misochko and P. H. M. van Loosdrecht, *Phys. Rev. B: Condens. Matter Mater. Phys.*, 2009, **80**, 161207(R).
47 R. P. Saichu, I. Mahns, A. Goos, S. Binder, P. May, S. G. Singer, B. Schulz, A. Rusydi, J. Unterhinninghofen, D. Manske, P. Guptasarma, M. S. Williamsen and M. Rübhausen, *Phys. Rev. Lett.*, 2009, **102**, 177004.
48 H. G. Yan, D. H. Song, K. F. Mak, I. Chatzakis, J. Maultzsch and T. F. Heinz, *Phys. Rev. B: Condens. Matter Mater. Phys.*, 2009, **80**, 12403.
49 J. M. Nesbitt and D. C. Smith, *Nano Lett.*, 2013, **13**, 416–422.
50 L. B. Gao, W. C. Ren, H. L. Xu, L. Jin, Z. X. Wang, T. Ma, L. P. Ma, Z. Y. Zhang, Q. Fu, L. M. Peng, X. H. Bao and H. M. Cheng, *Nat. Commun.*, 2012, **3**, 699.
51 Y. Wang, Y. Zheng, X. F. Xu, E. Dubuisson, Q. L. Bao, J. Lu and K. P. Loh, *ACS Nano*, 2011, **5**, 9927–9933.
52 B. V. Senkovskiy, A. V. Fedorov, D. Haberer, M. Farjam, K. A. Simonov, A. B. Preobrajenski, N. Martensson, N. Atodiresei, V. Caciuc, S. Blugel, A. Rosch, N. I. Verbitskiy, M. Hell, D. V. Evtushinsky, R. German, T. Marangoni, P. H. M. van Loosdrecht, F. R. Fischer and A. Grüneis, *Adv. Electron. Mater.*, 2017, **3**, 1600490.
53 R. B. Versteeg, J. Zhu, P. Padmanabhan, C. Boguschewski, R. German, M. Goedecke, P. Becker and P. H. M. van Loosdrecht, *Struct. Dyn.*, 2018, **5**, 044301.
54 K. Sasaki, K. Kato, Y. Tokura, S. Suzuki and T. Sogawa, *Phys. Rev. B: Condens. Matter Mater. Phys.*, 2012, **85**, 075437.
55 R. Gillen, M. Mohr and J. Maultzsch, *Phys. Status Solidi B*, 2010, **247**, 2941–2944.
56 H. Huang, D. C. Wei, J. T. Sun, S. L. Wong, Y. P. Feng, A. H. Castro Neto and A. T. S. Wee, *Sci. Rep.*, 2012, **2**, 983.
57 O. Deniz, C. Sánchez-Sánchez, T. Dumslaff, X. L. Feng, A. Narita, K. Müllen, N. Kharche, V. Meunier, R. Fasel and P. Ruffieux, *Nano Lett.*, 2017, **17**, 2197–2203.
58 K. Kang, D. Abdula, D. G. Cahill and M. Shim, *Phys. Rev. B: Condens. Matter Mater. Phys.*, 2010, **81**, 165405.
59 S. G. Chou, M. F. DeCamp, J. Jiang, G. G. Samsonidze, E. B. Barros, F. Plentz, A. Jorio, M. Zheng, G. B. Onoa, E. D. Semke, A. Tokmakoff, R. Saito, G. Dresselhaus and M. S. Dresselhaus, *Phys. Rev. B: Condens. Matter Mater. Phys.*, 2005, **72**, 195415.
60 D. J. Styers-Barnett, S. P. Ellison, C. Park, K. E. Wise and J. M. Papanikolas, *J. Phys. Chem. A*, 2005, **109**, 289–292.
61 D. J. Styers-Barnett, S. P. Ellison, B. P. Mehl, B. C. Westlake, R. L. House, C. Park, K. E. Wise and J. M. Papanikolas, *J. Phys. Chem. C*, 2008, **112**, 4507–4516.
62 O. A. Dyatlova, C. Köhler, E. Malic, J. Gomis-Bresco, J. Maultzsch, A. Tsagan-Mandzhiev, T. Watermann, A. Knorr and U. Woggon, *Nano Lett.*, 2012, **12**, 2249–2253.
63 R. C. Maher, J. Hou, L. F. Cohen, E. C. Le Ru, J. M. Hadfield, J. E. Harvey, P. G. Etchegoin, F. M. Liu, M. Green, R. J. Brown and M. J. Milton, *J. Chem. Phys.*, 2005, **123**, 084702.
64 R. C. Maher and L. F. Cohen, *J. Phys. Chem. A*, 2008, **112**, 1497–1501.
65 R. Loudon, *Adv. Phys.*, 1964, **13**, 423–482.
66 F. Wang, G. Dukovic, L. E. Brus and T. F. Heinz, *Phys. Rev. Lett.*, 2004, **92**, 177401.
67 H. B. Zhao and S. Mazumdar, *Phys. Rev. Lett.*, 2004, **93**, 157402.
68 R. M. Russo, E. J. Mele, C. L. Kane, I. V. Rubtsov, M. J. Therien and D. E. Luzzi, *Phys. Rev. B: Condens. Matter Mater. Phys.*, 2006, **74**, 041405.
69 J. Allam, M. T. Sajjad, R. Sutton, K. Litvinenko, Z. Wang, S. Siddique, Q. H. Yang, W. H. Loh and T. Brown, *Phys. Rev. Lett.*, 2013, **111**, 197401.
70 G. Soavi, F. Scotognella, D. Viola, T. Hefner, T. Hertel, G. Cerullo and G. Lanzani, *Sci. Rep.*, 2015, **5**, 9681.

